

Hydrogen-Bonded Liquid Crystal Elastomers Combining Shape Memory Programming and Reversible Actuation

Hongshuang Guo,* Tero-Petri Ruoko, Hao Zeng, and Arri Priimagi*

Materials that undergo shape morphing in response to external stimuli have numerous applications, e.g., in soft robotics and biomedical devices. Shape memory polymers utilize kinetically trapped states to, typically irreversibly, transfer between a programmed morphed shape and an equilibrium shape. Liquid crystal elastomers (LCEs), in turn, can undergo reversible actuation in response to several stimuli. This study combines the irreversible and reversible shape morphing processes to obtain LCEs that undergo shape-programming via the shape memory effect and subsequent reversible actuation of the programmed shape. This is enabled by an LCE crosslinked via dynamic hydrogen bonds that break at high temperatures and reform upon cooling, endowing the shape memory effect, while mild thermal or photothermal stimulation yields the reversible actuation. Through this combination, proof-of-concept robotic application scenarios such as grippers that can adjust their shape for grabbing different-sized objects and crawling robots that can morph their shape to adapt to constrained spaces, are demonstrated. It is anticipated that this work adds new diversity to shape-programmable soft microrobotics.

In soft robotics, shape-morphing materials are key components that enable characteristics such as navigation in complex environments and adaptation to tight spaces.^[21,22] In biomedical engineering, they serve as, e.g., shape-adjustable smart implants or expandable stents.^[23,24] Based on these examples, it is clear that shape-morphing materials open up new avenues for advanced technologies, and their potential applications are vast and varied.

Shape memory effect occurs when a material “memorizes” and recovers its original shape after being kinetically trapped in a deformed state through mechanical deformation.^[25–30] The effect is observed in different types of materials such as shape memory alloys^[31,32] and polymers exhibiting phase transitions or dynamic bonds.^[10,33,34] The shape recovery occurs in response to a specific stimulus such as temperature. The shape programming can be repeatedly conducted, typically at

elevated temperatures, followed by fixation of the kinetically trapped state(s) upon cooling. However, the shape memory effect typically proceeds one-way, from the kinetically trapped to the equilibrium state under a specific stimulus, leading to a one-time action in shape morphing.^[9,30,35–39]

Soft actuators undergoing reversible stimuli-induced movements are constructed from compliant, deformable, and elastic materials such as hydrogels^[40–43] or—particularly relevant for this work—liquid crystal elastomers (LCE).^[11–15,44,45] LCEs combine liquid crystal order and elastomeric properties in aligned, loosely crosslinked polymer networks and can undergo reversible deformations in response to various stimuli such as electric^[46] and magnetic fields,^[47] temperature,^[48] and light.^[49,50] The deformations are fast and precisely programmable via molecular alignment control during polymerization. LCEs also offer tunable mechanical properties such as stiffness and stretchability, which can be tailored by adjusting the molecular structure and crosslink density of the polymer network.^[51] The obtained movements can mimic the actions of natural muscles, allowing for bioinspired approaches in soft robotics applications.^[14,52,53] Due to their inherent compliance and deformability, LCEs are well-suited for applications where traditional rigid actuators may cause damage or discomfort, such as wearable medical devices or soft robotic exoskeletons.^[54,55] Another advantage, which differs them from conventional shape memory polymers, is their reversibility, meaning they can

1. Introduction

Soft materials with the ability to morph their shape in response to external stimuli have been extensively investigated during the past decade.^[1] Some examples of such materials are responsive hydrogels,^[2,3] dielectric elastomers,^[4,5] liquid crystal elastomers,^[6–8] and shape memory polymers,^[9,10] all of which can undergo different types of deformation, including bending, twisting, folding, and stretching, depending on the composition and fabrication details of the material used and the type of stimulus.^[11–17] These characteristics make them widely applicable in the fields of soft robotics and biomedical devices.^[18–20]

H. Guo, T.-P. Ruoko, H. Zeng, A. Priimagi
Smart Photonic Materials
Faculty of Engineering and Natural Sciences
Tampere University
Tampere FI-33101, Finland
E-mail: hongshuang.guo@tuni.fi; arri.priimagi@tuni.fi

The ORCID identification number(s) for the author(s) of this article can be found under <https://doi.org/10.1002/adfm.202312068>

© 2023 The Authors. Advanced Functional Materials published by Wiley-VCH GmbH. This is an open access article under the terms of the Creative Commons Attribution License, which permits use, distribution and reproduction in any medium, provided the original work is properly cited.

DOI: 10.1002/adfm.202312068

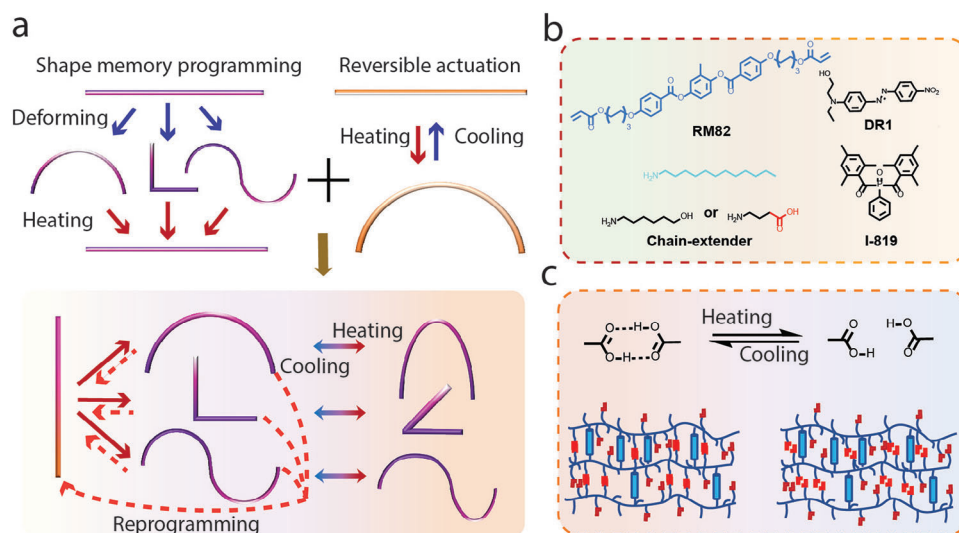


Figure 1. The design concept. a) Schematic illustration of shape-memory programming combined with reversible actuation. b) The chemical structures of the materials used. c) The shape-memory programming relies on hydrogen bond breaking and reforming upon heating and cooling, respectively.

be repeatedly activated and deactivated without losing their functionality.

In recent years, researchers have been exploring the potential of combining the pros of shape memory materials and soft actuators to create versatile devices with adaptable movements. One exciting development is the concept of two-way shape memory,^[9] where a material can be programmed to recover two different shapes depending on the stimulus applied.^[56] Another emerging concept is reconfigurable actuation where the actuator morphs into different shapes under an identical stimulus through an additional programming step.^[57–59] This can be achieved by using multi-material composites or by embedding different functional components into the actuator. Reconfigurable actuators have the potential to greatly expand the range of motions and functions that can be achieved in soft robotics and other applications.^[60] However, developing these materials and devices presents several challenges, such as the complexity of the chemistry involved and careful control over processing conditions and material properties.^[61] Additionally, integrating reconfigurable actuators into complex systems and controlling their behavior in functional devices remains a challenge.^[59]

In this article, a facile method to combine shape memory effect and reversible actuation within a single soft material is introduced. This is enabled by an LCE crosslinked via dynamic hydrogen bonds that break at high temperatures and reform upon cooling, endowing the shape memory effect, while mild thermal or photothermal stimulation of the LCE yields the reversible actuation. Various temporary shapes can be programmed into the material due to the shape-memory effect, and the temporary states can be further actuated using moderate heating or photothermal effect. The original state of the system can be restored by heating it to a sufficiently high temperature, allowing reprogramming of the material to a different temporary shape. The proposed LCE actuator can be accommodated to grip objects with different sizes and shapes, and for the design of shape-adjustable locomotors that move, e.g., in constrained spaces. The presented materi-

als concept points toward facile control and reconfiguration of responsive-materials-based, small-scale robotics.

2. Results and Discussion

2.1. The Design Concept

Our aim is to fabricate an actuator that can i) be programmed to various temporary shapes, ii) perform reversible (photo)actuation of the temporary shape, and iii) be restored to the original state and reprogrammed to a different temporary shape at will. To achieve this, we utilize the shape memory effect to allow the material to maintain the temporary shape, while LCE actuation provides the capability for reversible deformation.^[62] Traditional shape memory polymers cannot perform as reversible actuators because they rely on kinetically trapped states. In contrast, LCE actuators rapidly deform upon (photo)thermal stimulation and immediately return to the original shape when the energy source is removed. Hence, combining these two effects should allow combining (i)–(iii) through shape programming via the shape memory effect, and reversible shape morphing via the LCE actuation, as illustrated in **Figure 1a**.

Of the several methods to introduce shape memory function into LCEs,^[63–65] our approach is based on the incorporation of hydrogen bonds into a chain-extended LCE.^[11,66] The chain extension was conducted via the Aza–Michael addition reaction,^[11,67,68] as shown in Figure 1b and Figure S1a (Supporting Information). All experiments were conducted using surface aligned, splay-oriented LCE strips. Their preparation process and bending mechanism are depicted in Figure S1b,c (Supporting Information). To form the hydrogen-bonded network, alkylamine chain extenders were functionalized with carboxyl and hydroxyl groups. The corresponding LCEs, named LCE-COOH and LCE-OH, contain the functionalized chain extenders and dodecylamine in a 1:1 ratio, whereas an LCE with only dodecylamine chain extender (LCE-C₁₂; no ability to form hydrogen bonds) is used as a reference. The COOH groups are known to form

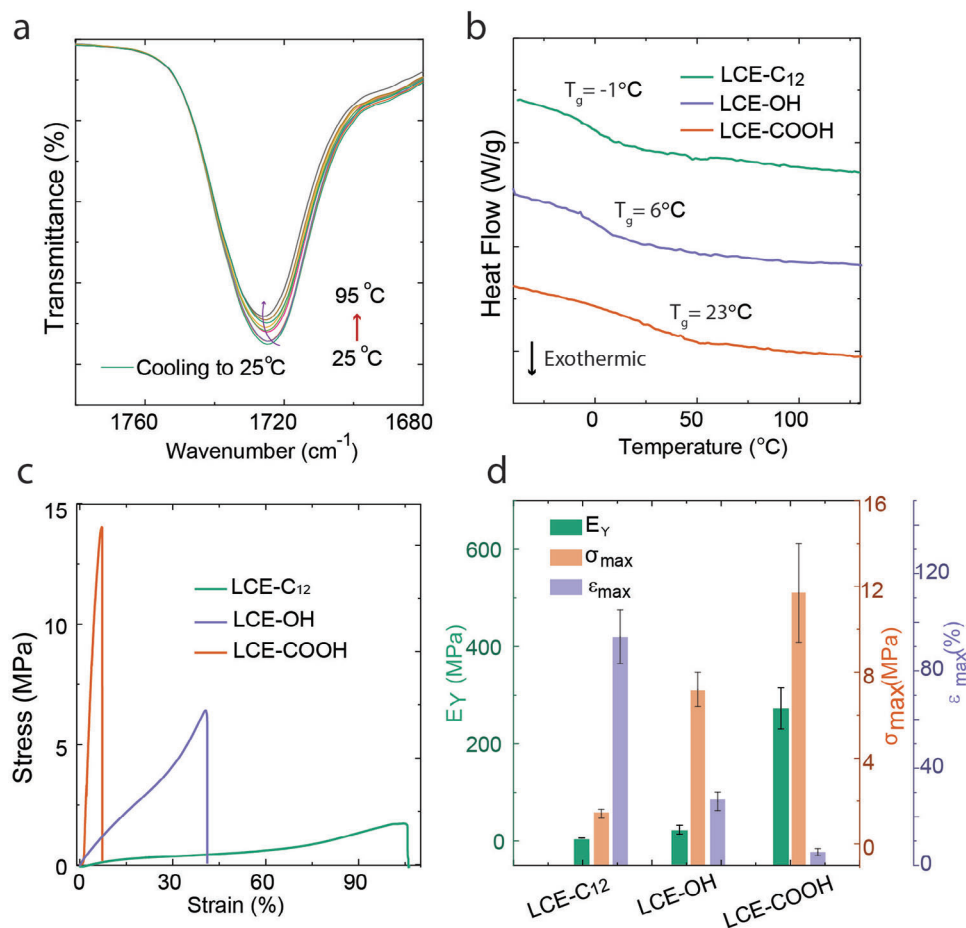


Figure 2. Material Characterization. a) Temperature-variable FTIR spectra of LCE-COOH upon heating from 25 to 95 °C (interval: 10 °C) and cooling back to 25 °C. b) DSC curves of LCE-C₁₂, LCE-OH, and LCE-COOH from the second heating cycle at a heating/cooling rate of 10 °C min⁻¹. c) Tensile stress–strain curves of LCE-C₁₂, LCE-OH and LCE-COOH. d) Young’s modulus (E_Y), fracture strain (ϵ_{\max}), and tensile strength (σ_{\max}) of LCE-C₁₂, LCE-OH, and LCE-COOH. The error bars represent the standard deviation obtained from $n = 3$ experiments.

relatively strong hydrogen-bonded dimers^[69–72] while the aliphatic hydroxyl groups are anticipated to form very weak contacts.^[73] Disperse Red 1 (DR1) was added to the polymerizable mixtures at 1 wt% concentration to enable photothermal actuation of the LCEs. The key design premise is that the hydrogen bonds break when heated to high enough temperatures and reform when cooled, locking the temporary shape in place (Figure 1c).^[74–76] We hypothesize that the temporary shape can still be reversibly actuated as long as the photothermal heating is mild enough not to break the hydrogen bonds.

2.2. Material Characterization

The Fourier transform infrared (FTIR) spectra of LCE-C₁₂, LCE-OH, and LCE-COOH are shown in Figure S2 (Supporting Information). Due to the presence of the hydroxy groups in LCE-OH, it has the signature broad absorption peak of –OH at 3400 cm⁻¹,^[66] which is not present in LCE-C₁₂ and LCE-COOH. The $\nu(\text{C}=\text{O})$ absorption bands in the 1780–1600 cm⁻¹ region are present in all three LCEs.^[13] However, the intensity and position of the $\nu(\text{C}=\text{O})$ peak of LCE-COOH is shifted downfield due to the formation

of hydrogen-bonded networks, as confirmed by temperature-variable FTIR analysis shown in Figure 2a. As the temperature increases from 25 to 95 °C, the peak of $\nu(\text{C}=\text{O})$ at 1724 cm⁻¹ shifts to a higher frequency (1727 cm⁻¹) which has been attributed to the breaking of the hydrogen bond.^[77]

Indirect evidence on the formation of the H-bonded network in LCE-COOH is also provided by differential scanning calorimetry (DSC) experiments. As shown in Figure 2b and Figure S3 (Supporting Information), the glass transition temperature (T_g) of LCE-COOH (23 °C) is significantly higher than that of LCE-OH (6 °C) or LCE-C₁₂ (–1 °C). This suggests much stronger supramolecular crosslinks through COOH dimerization as opposed to the anticipated weak OH...OH contacts. The presence of hydrogen bonds also alters the mechanical properties of the LCEs (Figures 2c and 2d), with Young’s modulus and tensile strength of LCE-COOH (272.9 MPa / 11.7 MPas) being significantly higher than those of LCE-OH (20.4 MPa / 7.2 MPas) and LCE-C₁₂ (2.5 MPa / 1.5 MPas). At the same time, the fracture strain is reduced from 94% (LCE-C₁₂) to 27.2% (LCE-OH) and 5.5% (LCE-COOH).

Due to pronounced mechanical stiffening upon hydrogen bond formation, unlike the other two LCEs, the LCE-COOH can jump when placed on a hot plate together with a small amount of

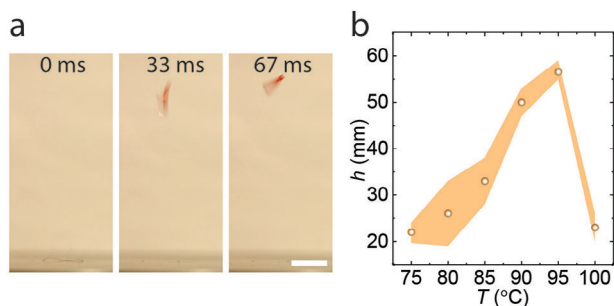


Figure 3. Jumping LCE. a) Snapshots of an LCE-COOH strip jumping on a 95 °C hot plate through releasing stored elastic energy. Scale bar: 1 cm. b) The jumping height of the LCE-COOH strip at different temperatures. The shaded area represents the standard deviation obtained from $n = 3$ experiments. Actuator dimensions: $10 \times 2 \times 0.1 \text{ mm}^3$.

water (Figure 3).^[78–80] When heated, the LCE-COOH strip tries to bend and stores energy due to the reduced molecular alignment, but still adheres to the hot plate due to the surface tension of the water. When the water evaporates, the stored energy is released, causing the strip to jump. As shown in Figure 3a,b and Movie S1 (Supporting Information), the maximum jumping height is observed at 95 °C. This can be attributed to the competition between the elastic energy-storing process during heating and the decrease in capillary force caused by water evaporation. Lower hot plate temperatures induce a smaller elastic strain and energy for jumping, whereas higher temperatures result in rapid evaporation of water, leading to a sudden drop of capillary adhesion before enough elastic energy can be stored. The mechanical stiffening is closely tied to enhanced material hardness and the subsequent rise in elastic potential energy. This can be elucidated by the increased elastic modulus, signifying the material's capacity to resist deformation in response to external forces. This augmented resistance necessitates the storage of elastic energy, representing the material's ability to promptly revert to its original shape post-deformation. Materials with higher mechanical hardness can accumulate more elastic energy, the release of which can lead to rapid, snap-through-type motions.^[81] Hence, LCE-COOH exhibits jumping motion (Figure 3) while under the experimental conditions used, its lower-modulus counterparts, LCE-OH and LCE-C₁₂, do not.

2.3. Shape Memory Programming and Reversible Actuation

Like any shape-memory material, the LCE-COOH can be programmed into different temporary shapes upon mechanical deformation at sufficiently high temperature, followed by cooling under stress. As shown in Figure 4a, the original shape can be restored when reheated to the programming temperature (100 °C). From the three LCEs studied, only LCE-COOH underwent the shape memory effect (Figure S4, Supporting Information). Reversible actuation of the shape-programmed LCE-COOH is illustrated in Figure 4b and Figure S5 (Supporting Information). The actuation direction can be controlled due to the splay alignment of the strip, leading to closing motion if the homeotropic side and opening if the planar side is on the outside, respectively. The maximum temperature for the thermally induced reversible actuation is limited by the temperature at which a large enough frac-

tion of the carboxylic dimers have opened up. In LCE-COOH this takes place when the temperature exceeds 50 °C, above which the material loses the programmed shape and returns to its original state (Figure S6). To avoid this, the experiments were conducted with 200 mW cm^{-2} light intensity, giving rise to photothermal heating to ca. 40 °C (Figure 4e). Higher light intensity, however, gives rise to higher surface temperature and hence larger bending curvature (Figure 4e; Figure S7, Supporting Information). We also note that the deformation of LCE-COOH under both thermal (Figure 4c) and photothermal (Figure 4d) stimulus is much less pronounced than for LCE-OH, due to the mechanical stiffening caused by hydrogen bonding (Figure 2c). In addition, the thickness of the LCE strip greatly influences the actuation speed, increasing thickness leading to slower material movement. This is illustrated in Figure S8a (Supporting Information), showing that the bending speeds for 100, 50, and 20 μm LCE-COOH strips are ca. 3.1, 1.6, and 0.9 s, respectively. Thinner strips also exhibit faster recovery speeds due to enhanced heat dissipation (Figure S8b, Supporting Information). However, it is essential to note that while thinner strips exhibit faster response speed, as a trade-off they generate smaller forces and may exhibit reduced stability during shape-memory programming. Therefore, for all subsequent experiments, LCE strips with a thickness of 100 μm were used.

2.4. Gripping and Locomotion

To demonstrate the utility of the proposed programming concept in small-scale soft robotics, we present two proof of concepts (Figure 5). The first one is a gripper (Figure 5a; Movie S2, Supporting Information) whose initial shape can be changed to fit objects of different sizes. The gripper can be opened via photothermal actuation to grab the object, and it closes once the photothermal stimulus is removed. The object remains captured in the dark and can be released under similar irradiation conditions. Although several gripper designs with sufficient bending for gripping action under light irradiation have been reported,^[58,82,83] increased light intensity tends to soften the material, resulting in lower force generation to grasp the object. The strength of the present design is the relatively low photothermal heating and most of all the fact that the gripping function remains after the illumination is ceased. Figure 5b demonstrates a crawling LCE locomotor (see also Movie S3, Supporting Information) which, in order to move, requires frictional force asymmetry between the front and back feet.^[84,85] The usual solution is to encode the friction bias either on both sides of the crawler or to use ratcheted surfaces.^[86–88] In the present design, this is achieved by programming the shape of the actuator strip, resulting in the required friction anisotropy for inducing net movement. After changing the actuator geometry that affects the contacting angle between the strip and the surface, the crawling speed of the robot increases (Figure S9a,b, Supporting Information). The walking trajectories of the differently shaped locomotors are further quantified in Figure S10a–c and Movie S4 (Supporting Information), where we fixed the light source and controlled the on-off switching in cycles consisting of 20 s irradiation followed by 20 s of darkness. It is evident that the movement speed of the strip with temporary shape 2 is significantly higher than the one with

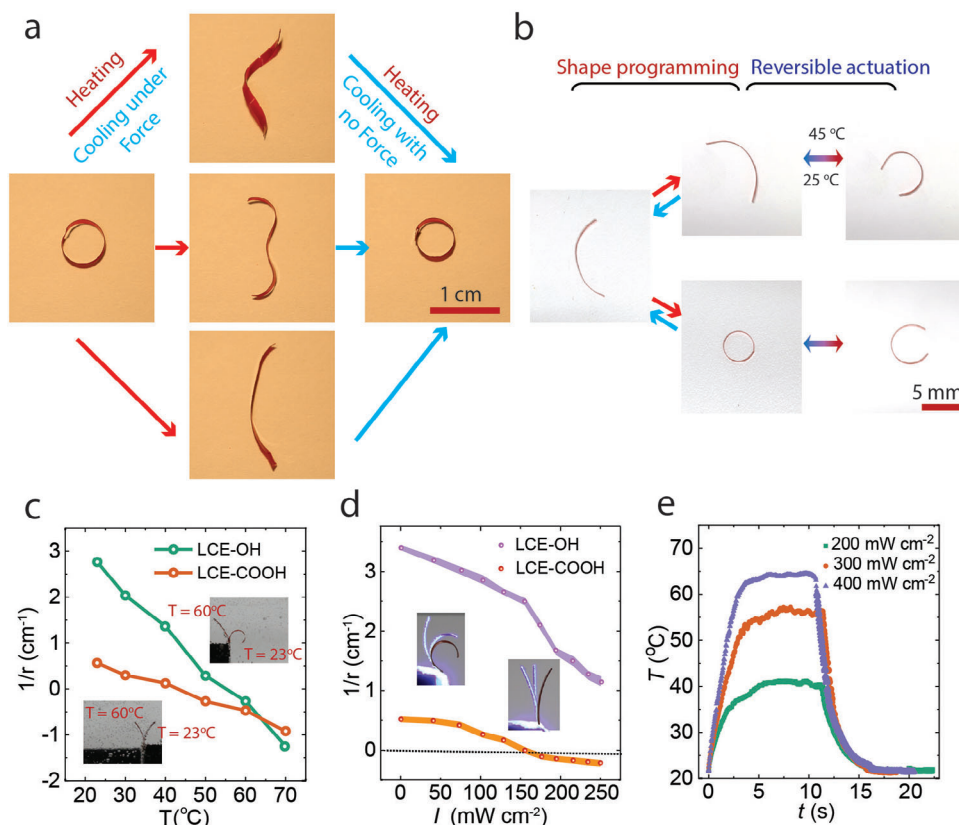


Figure 4. Shape memory programming and reversible actuation. a) Shape memory programming of LCE-COOH upon mechanical deformation at 100 °C and subsequent cooling to room temperature. The original shape can be retained upon re-heating. b) Reversible actuation of a shape-memory-programmed LCE-COOH strip under mild heating. The splay-aligned strip can be programmed to either bend or unbend upon heating. c) Temperature-induced bending of splay-aligned LCE-COOH and LCE-OH strips. Insets illustrate the bending process. d) Photothermally induced bending of splay-aligned LCE-COOH and LCE-OH strips. The shaded area represents the standard deviation of $n = 3$ measurements. Insets illustrate the bending process. e) Light-induced heating kinetics of LCE-COOH strip upon 460 nm illumination at different intensities. All strip sizes are $12 \times 2 \times 0.1 \text{ mm}^3$.

temporary shape 1. We note, however, that as the forward motion of the walking robot is controlled by varying friction through shape programming, not by altering surface roughness, the movement speed for both shapes is relatively slow. The shape of the locomotor can also be accommodated to fit inside confined spaces such as glass tubes (Figure 5b; Figure S9c, Supporting Information). A flat temporary state, in turn, facilitates movement through a narrow pathway, and after making its way through, the original curved actuator profile can be restored (Figure S11), attesting the utility of the concept of combining shape-memory programming and reversible actuation in facilitating movement through tight spaces.^[30]

3. Conclusion

We have shown that by incorporating dynamic hydrogen-bond crosslinks into Aza-Michael addition-based, chain-extended LCEs, it is possible to combine shape programming through the shape memory effect, and reversible actuation through LCE (photo)actuation. This is enabled by the incorporation of carboxylic acid groups that dimerize via hydrogen bonding,^[89] while hydroxy groups do not provide sufficiently strong bonds

to support the shape memory effect. The introduction of the supramolecular crosslinks enhances the mechanical properties of the LCE and endows it with the shape memory function while maintaining the ability to undergo reversible photothermal actuation under mild temperature stimulation. Compared to previous studies employing carboxylic acid-containing LCEs as base-treated salts,^[13,71,90,91] the preservation of the carboxylic dimers and their dynamic bonding properties is critical for our approach to work. The programmable actuator is further utilized as a light-controlled gripper whose shape can be accommodated to fit the size of the object, and as a reconfigurable crawling robot that can be adjusted in shape to fit different confined spaces. We believe that the method presented, combining (re)programmable shape, reversible (photo)actuation, and environmental adaptability may add new diversity for the future development of responsive-materials-based actuators and small-scale soft robots.

4. Experimental Section

Materials: 1,4-Bis-[4-(6-acryloyloxyhexyloxy)benzoyloxy]-2-methylbenzene (99%, RM82) was purchased from SYNTHON Chemicals GmbH

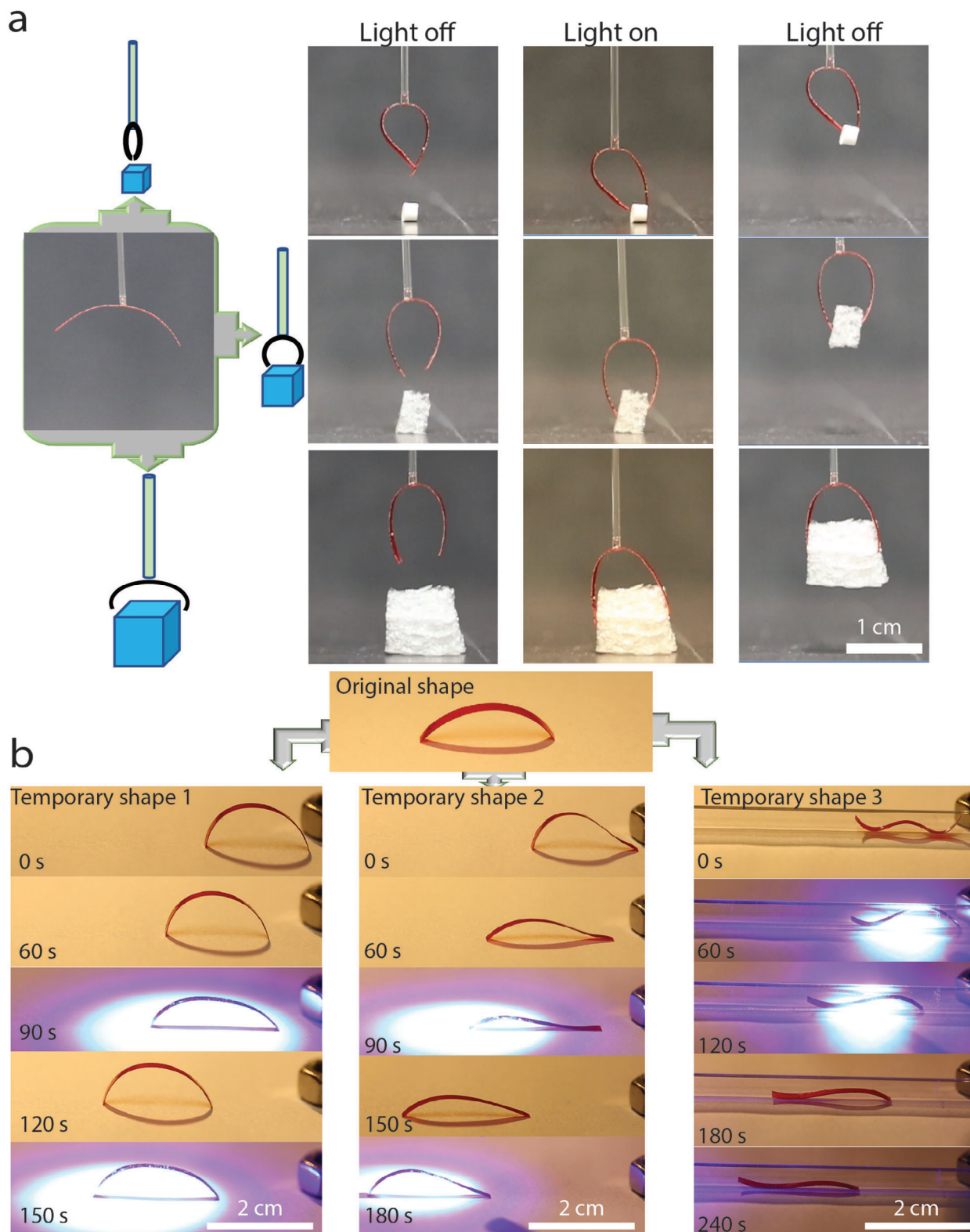


Figure 5. Gripping and locomotion. a) A light-controlled gripper with different temporary shapes. The figures demonstrate the use of the same gripper programmed to grab different-sized objects. b) A crawling robot with changeable initial shape. The figures illustrate locomotion on a piece of paper or inside a tube. Irradiation conditions 460 nm, 200 mW cm^{-2} . All strip sizes are $24 \times 2 \times 0.1 \text{ mm}^3$.

& Co. Disperse Red 1 was purchased from Merck. 6-Amino-1-hexanol, dodecylamine, phenylbis(2,4,6-trimethylbenzoyl)phosphine oxide (I-819) and γ -aminobutyric acid were purchased from TCI. All chemicals were used as received.

LCE Film Preparation: Two coated glass substrates were glued together to form LC cells. One slide was coated with a homeotropic alignment layer (JSR OPTMER, 4000 RPM for 1 min, followed by baking at 100 °C for 10 min and 180 °C for 30 min) and the other with rubbed polyvinyl alcohol (PVA, 5% water solution, 4000 RPM for 1 min, and baked at 100 °C for 10 min). 100 μ m microspheres (Thermo scientific) serve as spacers to determine the thickness of the LCE strips.

For LCE-OH and LCE-COOH, liquid crystal mixtures were prepared by mixing 0.14 mmol RM82, 0.06 mmol dodecylamine, 0.06 mmol 6-Amino-1-hexanol or γ -aminobutyric acid, 1.0 wt% Disperse Red 1, and 2.0 wt% of I-819. For LCE-C₁₂, the corresponding mixture contained 0.14 mmol RM82 and 0.12 mmol dodecylamine. The mixtures were filled into the LC cells via capillary effect at 100 °C and cooled down to 63 °C (1 °C min⁻¹). The cells were put in an oven to allow the Aza–Michael addition reaction for oligomerization for 24 h at 63 °C, followed by polymerization under UV light (380 nm, 180 mW cm⁻², 30 min). Finally, the cells were opened with a blade and strips with desired dimensions were cut from the film.

Material Characterization: The Fourier Transform Infrared (FTIR) spectra were recorded on a Perkin Elmer Spectrum Two spectrometer between 4000–650 cm⁻¹ with a clean ATR crystal used as reference. Differential Scanning Calorimetry (DSC) measurements were performed with a Netzsch DSC 214 Polyma instrument at a heating/cooling rate of 10 °C min⁻¹. The measurements were performed with 6–10 mg of sample at 1 bar under nitrogen atmosphere (flow rate of 20 mL min⁻¹) in the temperature range between –50 and 150 °C. Stress–strain curves were determined with a homemade tensile tester from 0.1 mm thick films with a stretching speed of 0.05 mm s⁻¹.

Optical Characterization: Canon 5D Mark III camera with 100 mm lens was used to capture optical images and relevant research videos. Thermal images were captured using an infrared camera with a close-up (2) lens (FLIR T420BX). CoolLED pE-4000 was used in this project for photopolymerization, actuation, and isomerization of the LCE films. A video analysis software was used to analyze the related data (Kinovea).

Supporting Information

Supporting Information is available from the Wiley Online Library or from the author.

Acknowledgements

A.P. gratefully acknowledges the financial support of the European Research Council (Consolidator Grant project MULTIMODAL; Agreement No. 101045223). The authors acknowledge financial support from the Academy of Finland, provided through Academy Postdoctoral Researcher projects No. 347201 for H.G. and No. 340103 for T.P.R. and Academy Research Fellowship No. 340263 for H.Z. This work was conducted as part of the Academy of Finland Center of Excellence “Life-Inspired Hybrid Materials Research” (LIBER, No. 346107) and the Academy of Finland Flagship Programme on Photonics Research and Innovation (PREIN, No. 320165). T.P.R. acknowledges the European Union’s Horizon 2020 research and innovation programme under the Marie Skłodowska-Curie grant agreement No. 101022777.

Conflict of Interest

The authors declare no conflict of interest.

Data Availability Statement

The data that support the findings of this study are available from the corresponding author upon reasonable request.

Keywords

hydrogen bond, liquid crystal elastomer, microrobot, photoactuation, shape memory

Received: October 2, 2023

Revised: November 14, 2023

Published online:

- [1] J. M. Mccracken, B. R. Donovan, T. J. White, *Adv. Mater.* **2020**, *32*, 1906564.
- [2] S.-J. Jeon, A. W. Hauser, R. C. Hayward, *Acc. Chem. Res.* **2017**, *50*, 161.
- [3] X. Liu, M. Gao, J. Chen, S. Guo, W. Zhu, L. Bai, W. Zhai, H. Du, H. Wu, C. Yan, Y. Shi, J. Gu, H. J. Qi, K. Zhou, *Adv. Funct. Mater.* **2022**, *32*, 2203323.
- [4] Y. Shi, E. Askounis, R. Plamthottam, T. Libby, Z. Peng, K. Youssef, J. Pu, R. Pelrine, Q. Pei, *Science* **2022**, *377*, 228.
- [5] J. Pu, Y. Meng, Z. Xie, Z. Peng, J. Wu, Y. Shi, R. Plamthottam, W. Yang, Q. Pei, *Sci. Adv.* **2022**, *8*, eabm6200.
- [6] T. J. White, D. J. Broer, *Nat. Mater.* **2015**, *14*, 1087.
- [7] T. Guin, M. J. Settle, B. A. Kowalski, A. D. Auguste, R. V. Beblo, G. W. Reich, T. J. White, *Nat. Commun.* **2018**, *9*, 2531.
- [8] Q. He, Z. Wang, Y. Wang, Z. Wang, C. Li, R. Annapooranan, J. Zeng, R. Chen, S. Cai, *Sci. Robot.* **2021**, *6*, eabi9704.
- [9] A. Lendlein, O. E. C. Gould, *Nat. Rev. Mater.* **2019**, *4*, 116.
- [10] Y. Xia, Y. He, F. Zhang, Y. Liu, J. Leng, *Adv. Mater.* **2021**, *33*, 2000713.
- [11] T. H. Ware, M. E. Mcconney, J. J. Wie, V. P. Tondiglia, T. J. White, *Science* **2015**, *347*, 982.
- [12] H.-F. Lu, M. Wang, X.-M. Chen, B.-P. Lin, H. Yang, *J. Am. Chem. Soc.* **2019**, *141*, 14364.
- [13] O. M. Wani, R. Verpaalen, H. Zeng, A. Priimagi, A. P. H. J. Schenning, *Adv. Mater.* **2019**, *31*, 1805985.
- [14] Y. Zhang, Z. Wang, Y. Yang, Q. Chen, X. Qian, Y. Wu, H. Liang, Y. Xu, Y. Wei, Y. Ji, *Sci. Adv.* **2020**, *6*, eaay8606.
- [15] S. Iamsaard, S. J. Aßhoff, B. Matt, T. Kudernac, J. J. L. M. Cornelissen, S. P. Fletcher, N. Katsonis, *Nat. Chem.* **2014**, *6*, 229.
- [16] X. Zhang, Z. Yu, C. Wang, D. Zarrouk, J.-W. T. Seo, J. C. Cheng, A. D. Buchan, K. Takei, Y. Zhao, J. W. Ager, J. Zhang, M. Hettick, M. C. Hersam, A. P. Pisano, R. S. Fearing, A. Javey, *Nat. Commun.* **2014**, *5*, 2983.
- [17] C. Li, Y. Xue, M. Han, L. C. Palmer, J. A. Rogers, Y. Huang, S. I. Stupp, *Matter* **2021**, *4*, 1377.
- [18] Z. Li, N. V. Myung, Y. Yin, *Sci. Robot.* **2021**, *6*, eabi4523.
- [19] H. Kim, S.-K. Ahn, D. M. Mackie, J. Kwon, S. H. Kim, C. Choi, Y. H. Moon, H. B. Lee, S. H. Ko, *Mater. Today* **2020**, *41*, 243.
- [20] J. Delaey, P. Dubruel, S. Van Vlierberghe, *Adv. Funct. Mater.* **2020**, *30*, 1909047.
- [21] D. S. Shah, J. P. Powers, L. G. Tilton, S. Kriegman, J. Bongard, R. Kramer-Bottiglio, *Nat. Mach. Intell.* **2021**, *3*, 51.
- [22] D. Shah, B. Yang, S. Kriegman, M. Levin, J. Bongard, R. Kramer-Bottiglio, *Adv. Mater.* **2021**, *33*, 2002882.
- [23] X. Liu, C. Steiger, S. Lin, G. A. Parada, J. Liu, H. F. Chan, H. Yuk, N. V. Phan, J. Collins, S. Tamang, G. Traverso, X. Zhao, *Nat. Commun.* **2019**, *10*, 493.
- [24] X. Chen, B. Assadsangabi, Y. Hsiang, K. Takahata, *Adv. Sci.* **2018**, *5*, 1700560.
- [25] Q. Zhao, W. Zou, Y. Luo, T. Xie, *Sci. Adv.* **2016**, *2*, 1501297.
- [26] T. Xie, *Nature* **2010**, *464*, 267.
- [27] J. Meurer, J. Hniopek, T. Bätz, S. Zechel, M. Enke, J. Vitz, M. Schmitt, J. Popp, M. D. Hager, U. S. Schubert, *Adv. Mater.* **2021**, *33*, 2006655.
- [28] W. Miao, W. Zou, B. Jin, C. Ni, N. Zheng, Q. Zhao, T. Xie, *Nat. Commun.* **2020**, *11*, 4257.

- [29] B. Zhang, H. Li, J. Cheng, H. Ye, A. H. Sakhaei, C. Yuan, P. Rao, Y.-F. Zhang, Z. Chen, R. Wang, X. He, J. Liu, R. Xiao, S. Qu, Q. Ge, *Adv. Mater.* **2021**, *33*, 2101298.
- [30] B. Jin, H. Song, R. Jiang, J. Song, Q. Zhao, T. Xie, *Sci. Adv.* **2018**, *4*, eaao3865.
- [31] P. Chowdhury, H. Sehitoglu, *Prog. Mater. Sci.* **2017**, *88*, 49.
- [32] F. A. Hassani, W. Y. X. Peh, G. G. L. Gammad, R. P. Mogan, T. K. Ng, T. L. C. Kuo, L. G. Ng, P. Luu, S.-C. Yen, C. Lee, *Adv. Sci.* **2017**, *4*, 1700143.
- [33] H. Guo, R. Puttreddy, T. Salminen, A. Lends, K. Jaudzems, H. Zeng, A. Priimagi, *Nat. Commun.* **2022**, *13*, 7436.
- [34] L. Yang, G. Zhang, N. Zheng, Q. Zhao, T. Xie, *Angew. Chem., Int. Ed.* **2017**, *56*, 12599.
- [35] C. N. Zhu, T. Bai, H. Wang, J. Ling, F. Huang, W. Hong, Q. Zheng, Z. L. Wu, *Adv. Mater.* **2021**, *33*, 2102023.
- [36] H. Ur Rehman, Y. Chen, M. S. Hedenqvist, H. Li, W. Xue, Y. Guo, Y. Guo, H. Duan, H. Liu, *Adv. Funct. Mater.* **2018**, *28*, 1704109.
- [37] S.-Y. Leo, Y. Ni, C. Xu, Y. Zhang, Y. Dai, P. Qi, A. T. Xie, V. Basile, C. Taylor, P. Jiang, *Adv. Funct. Mater.* **2017**, *27*, 1703522.
- [38] X. Wang, X. Guo, J. Ye, N. Zheng, P. Kohli, D. Choi, Y. Zhang, Z. Xie, Q. Zhang, H. Luan, K. Nan, B. H. Kim, Y. Xu, X. Shan, W. Bai, R. Sun, Z. Wang, H. Jang, F. Zhang, Y. Ma, Z. Xu, X. Feng, T. Xie, Y. Huang, Y. Zhang, J. A. Rogers, *Adv. Mater.* **2019**, *31*, 1805615.
- [39] H. Lu, B. Wu, X. Le, W. Lu, Q. Yang, Q. Liu, J. Zhang, T. Chen, *Adv. Funct. Mater.* **2022**, *32*, 2206912.
- [40] H. Na, Y.-W. Kang, C. S. Park, S. Jung, H.-Y. Kim, J.-Y. Sun, *Science* **2022**, *376*, 301.
- [41] A. K. Mishra, T. J. Wallin, W. Pan, P. Xu, K. Wang, E. P. Giannelis, B. Mazzolai, R. F. Shepherd, *Sci. Robot.* **2020**, *5*, eaaz3918.
- [42] Z. Jiang, M. L. Tan, M. Taheri, Q. Yan, T. Tsuzuki, M. G. Gardiner, B. Diggie, L. A. Connal, *Angew. Chem., Int. Ed.* **2020**, *59*, 7049.
- [43] A. Paikar, A. I. Novichkov, A. I. Hanopolskyi, V. A. Smaliak, X. Sui, N. Kampf, E. V. Skorb, S. N. Semenov, *Adv. Mater.* **2022**, *34*, 2106816.
- [44] K. M. Herbert, H. E. Fowler, J. M. Mccracken, K. R. Schlafmann, J. A. Koch, T. J. White, *Nat. Rev. Mater.* **2022**, *7*, 23.
- [45] O. M. Wani, H. Zeng, A. Priimagi, *Nat. Commun.* **2017**, *8*, 15546.
- [46] Q. He, Z. Wang, Y. Wang, A. Minori, M. T. Tolley, S. Cai, *Sci. Adv.* **2019**, *5*, eaax5746.
- [47] W. Hu, G. Z. Lum, M. Mastrangeli, M. Sitti, *Nature* **2018**, *554*, 81.
- [48] Y. Zhao, Y. Hong, F. Qi, Y. Chi, H. Su, J. Yin, *Adv. Mater.* **2023**, *35*, 2207372.
- [49] Z. Hu, Y. Li, J.-A. Lv, *Nat. Commun.* **2021**, *12*, 3211.
- [50] A. H. Gelebart, D. Jan Mulder, M. Varga, A. Konya, G. Vantomme, E. W. Meijer, R. L. B. Selinger, D. J. Broer, *Nature* **2017**, *546*, 632.
- [51] X. Lin, W. Zou, E. M. Terentjev, *Macromolecules* **2022**, *55*, 810.
- [52] A. Kotikian, J. M. Morales, A. Lu, J. Mueller, Z. S. Davidson, J. W. Boley, J. A. Lewis, *Adv. Mater.* **2021**, *33*, 2101814.
- [53] A. Kotikian, C. McMahan, E. C. Davidson, J. M. Muhammad, R. D. Weeks, C. Daraio, J. A. Lewis, *Sci. Robot.* **2019**, *4*, eaax7044.
- [54] J. Xiong, J. Chen, P. S. Lee, *Adv. Mater.* **2021**, *33*, 2002640.
- [55] C. P. Ambulo, S. Tasmim, S. Wang, M. K. Abdelrahman, P. E. Zimmern, T. H. Ware, *J. Appl. Phys.* **2020**, *128*, 140901.
- [56] G. Chen, J. Dong, X. Xu, W. Zou, B. Jin, W. Peng, Q. Zhao, T. Xie, N. Zheng, *J. Mater. Chem. A* **2022**, *10*, 10350.
- [57] J. Jiang, L. Han, F. Ge, Y. Xiao, R. Cheng, X. Tong, Y. Zhao, *Angew. Chem., Int. Ed.* **2022**, *61*, 202116689.
- [58] M. Lahikainen, H. Zeng, A. Priimagi, *Nat. Commun.* **2018**, *9*, 4148.
- [59] M. Zhang, H. Shahsavan, Y. Guo, A. Pena-Francesch, Y. Zhang, M. Sitti, *Adv. Mater.* **2021**, *33*, 2008605.
- [60] R. Khodambashi, Y. Alsaïd, R. Rico, H. Marvi, M. M. Peet, R. E. Fisher, S. Berman, X. He, D. M. Aukes, *Adv. Mater.* **2021**, *33*, 2005906.
- [61] M. Li, T. Kim, G. Guidetti, Y. Wang, F. G. Omenetto, *Adv. Mater.* **2020**, *32*, 2004147.
- [62] M. Behl, M. Y. Razaq, A. Lendlein, *Adv. Mater.* **2010**, *22*, 3388.
- [63] E. C. Davidson, A. Kotikian, S. Li, J. Aizenberg, J. A. Lewis, *Adv. Mater.* **2020**, *32*, 1905682.
- [64] K. M. Lee, H. Koerner, R. A. Vaia, T. J. Bunning, T. J. White, *Soft Matter* **2011**, *7*, 4318.
- [65] S.-K. Ahn, R. M. Kasi, *Adv. Funct. Mater.* **2011**, *21*, 4543.
- [66] H.-H. Yoon, D.-Y. Kim, K.-U. Jeong, S.-K. Ahn, *Macromolecules* **2018**, *51*, 1141.
- [67] A. Kotikian, R. L. Truby, J. W. Boley, T. J. White, J. A. Lewis, *Adv. Mater.* **2018**, *30*, 1706164.
- [68] W. Zou, X. Lin, E. M. Terentjev, *Adv. Mater.* **2021**, *33*, 2101955.
- [69] K. R. Schlafmann, M. S. Alahmed, K. L. Lewis, T. J. White, *Adv. Funct. Mater.* **2023**, 2305818, <https://doi.org/10.1002/adfm.202305818>.
- [70] K. L. Lewis, K. M. Herbert, V. M. Mataulij, J. D. Hoang, E. T. Ellison, G. E. Bauman, J. A. Herman, T. J. White, *ACS Appl. Mater. Interfaces* **2023**, *15*, 3467.
- [71] L. T. De Haan, J. M. N. Verjans, D. J. Broer, C. W. M. Bastiaansen, A. P. H. J. Schenning, *J. Am. Chem. Soc.* **2014**, *136*, 10585.
- [72] Y. Foelen, D. A. C. Van Der Heijden, A. M. J. Verdurmen, D. J. Mulder, J. Lub, A. P. H. J. Schenning, *Adv. Opt. Mater.* **2022**, *10*, 2201462.
- [73] G. Gilli, P. Gilli, *The Nature of the Hydrogen Bond: Outline of a Comprehensive Hydrogen Bond Theory*, Oxford University Press, Oxford, England **2009**.
- [74] Y. Shen, B. Wang, D. Li, X. Xu, Y. Liu, Y. Huang, Z. Hu, *Polym. Chem.* **2022**, *13*, 1130.
- [75] T. Ware, K. Hearon, A. Lonneck, K. L. Wooley, D. J. Maitland, W. Voit, *Macromolecules* **2012**, *45*, 1062.
- [76] J. Uchida, M. Yoshio, T. Kato, *Chem. Sci.* **2021**, *12*, 6091.
- [77] K. D. Harris, C. W. M. Bastiaansen, J. Lub, D. J. Broer, *Nano Lett.* **2005**, *5*, 1857.
- [78] T. S. Hebnar, K. Korner, C. N. Bowman, K. Bhattacharya, T. J. White, *Sci. Adv.* **2023**, *9*, eade1320.
- [79] J. Hu, Z. Nie, M. Wang, Z. Liu, S. Huang, H. Yang, *Angew. Chem., Int. Ed.* **2023**, *135*, 202218227.
- [80] J. Wang, T. Zhao, Y. Fan, H. Wu, J.-A. Lv, *Adv. Funct. Mater.* **2023**, *33*, 2209798.
- [81] M. F. Ashby, D. R. Jones, *Engineering materials 1: an introduction to properties, applications and design*, 4th ed., Elsevier, Amsterdam, Netherlands **2012**, Vol. 1.
- [82] Y.-Y. Xiao, Z.-C. Jiang, X. Tong, Y. Zhao, *Adv. Mater.* **2019**, *31*, 1903452.
- [83] M. Pilz Da Cunha, Y. Foelen, R. J. H. Van Raak, J. N. Murphy, T. A. P. Engels, M. G. Debije, A. P. H. J. Schenning, *Adv. Opt. Mater.* **2019**, *7*, 1801643.
- [84] G. Gao, Z. Wang, D. Xu, L. Wang, T. Xu, H. Zhang, J. Chen, J. Fu, *ACS Appl. Mater. Interfaces* **2018**, *10*, 41724.
- [85] Y. S. Kim, M. Liu, Y. Ishida, Y. Ebina, M. Osada, T. Sasaki, T. Hikima, M. Takata, T. Aida, *Nat. Mater.* **2015**, *14*, 1002.
- [86] Y. Wang, R. Yin, L. Jin, M. Liu, Y. Gao, J. Raney, S. Yang, *Adv. Funct. Mater.* **2023**, *33*, 2210614.
- [87] Y. Wu, J. K. Yim, J. Liang, Z. Shao, M. Qi, J. Zhong, Z. Luo, X. Yan, M. Zhang, X. Wang, R. S. Fearing, R. J. Full, L. Lin, *Sci. Robot.* **2019**, *4*, eaax1594.
- [88] Y. Tang, Y. Chi, J. Sun, T.-H. Huang, O. H. Maghsoudi, A. Spence, J. Zhao, H. Su, J. Yin, *Sci. Adv.* **2020**, *6*, eaaz6912.
- [89] S. J. D. Luggar, S. J. A. Houben, Y. Foelen, M. G. Debije, A. P. H. J. Schenning, D. J. Mulder, *Chem. Rev.* **2022**, *122*, 4946.
- [90] A. Ryabchun, F. Lancia, A.-D. Nguindjel, N. Katsonis, *Soft Matter* **2017**, *13*, 8070.
- [91] R. Lan, J. Sun, C. Shen, R. Huang, L. Zhang, H. Yang, *Adv. Funct. Mater.* **2019**, *29*, 1900013.